Pressure and diffusion of active matter with inertia

Mario Sandoval [*]

Department of Physics, Universidad Autonoma Metropolitana-Iztapalapa, Mexico City 09340, Mexico

(Received 22 September 2019; revised manuscript received 17 November 2019; published 23 January 2020)

It has been discovered that active matter generates novel physical quantities such as the swim pressure. This quantity arises from the exchange of extra momentum between active particles and the boundaries of the system. Given its origin, this quantity can exist at different scales; hence microorganisms and larger organisms like fish or birds generate their own swim pressure. For larger organisms or for high swimming speeds, inertia cannot necessarily be neglected; hence in this paper, we start by calculating analytically the effect of finite translational and rotational particles' inertia on the diffusion of a system of noninteracting spherical active Brownian particles. From this analysis, an enhanced diffusion coefficient due to rotational inertia is obtained, and an alternative effective persistence length and an alternative reorientation time, both sensitive to rotational inertia, are also identified. Afterwards, and to see the implications of finite inertia on bulk properties, the pressure of this system is elucidated by calculating its respective swim and Reynolds pressures. It is found that their sum becomes asymptotically sensitive to the square root of its rotational inertia. To validate our analytical results, Langevin dynamics simulations are also performed showing an excellent agreement between our theoretical predictions and the numerical results.

DOI: 10.1103/PhysRevE.101.012606

I. INTRODUCTION

The study of active matter constituted of natural or artificial entities able to self-propel is being widely engaged in [1–5]. For example, active systems are being considered as minimal models able to provide insight on phase transitions and self-assembly in nonequilibrium systems [6–10]. Micro- and nanomachines capable of self-propelling inside the human body and used to accomplish certain biomedical applications are already being tested [11]. In addition, efforts to understand the motion of microorganisms (which are an example of natural self-propelled entities), their wall accumulation, the effects of external fields on their motion, and their collective effects are also being carried out [12].

Quite recently, it was discovered that active matter generates novel physical quantities like the swim pressure [9,13,14]. Physically, this quantity arises from the exchange of extra momentum (due to self-propulsion) between an active particle and the boundaries of the system. Given its origin, this quantity can exist at different scales; hence microorganisms and larger organisms like fish or birds generate their own swim pressure. The swim pressure has already been used to explain phase separation in a system of interacting active particles. For example, Takatori *et al.* [9] identified an active pressure-volume phase diagram very similar to that of a van der Waals fluid and found related arguments like those from classical thermodynamics to explain phase transitions in active matter. Moreover, using this active pressure concept, analogous expressions for thermodynamiclike constructions like the chemical potential, Helmholtz free energy, and spinodal and binodal lines have been introduced and successfully used to understand phase transitions in active matter [14].

As one can see, the majority of active matter studies consider the overdamped approximation; that is, translational and rotational inertia are neglected. Would inertia play a role in active systems? What could happen if the system of interest consists of larger individuals or higher swimming speeds where inertia cannot be neglected? Since typical models for active systems couple translation and rotation [15], one has the possibility that this coupling together with inertia may indeed affect the system's properties, like its diffusion and pressure. These questions are discussed in the present paper, particularly, the effects of inertia on the diffusion and the swim and Reynolds pressures of a system of spherical noninteracting active Brownian particles (ABPs) are addressed. In the literature dealing with the calculation of pressure in a system of ABPs [6,13,16–19], only a few works have included inertia in their studies. One example is Joyeux and Bertin [20] who studied a dumbbell gas with only translational inertia and found its effective pressure. Takatori and Brady [21] considered the effect of translational inertia on the pressure of a system of ABPs in a suspension and found that the system's swim pressure is sensitive to it. They also identified a contribution to the total pressure of the system, the Reynolds pressure, which originates from the fact that particles have finite inertia. They concluded that although such pressures are sensitive to translational inertia, their sum becomes independent from translational inertia. Fily *et al.* [22] also considered an underdamped dynamics (only in translation) for ABPs to discuss the existence of an equation of state. A recent work providing a system (active vibrobots) where one can perform experimental studies to verify our presented theory has also been reported [23].

[*] sem@xanum.uam.mx

Furthermore, given the fact that the total active pressure has been proved to explain transitions in active matter; there is a need to extend previous works to the case of active systems with inertia and then to use those findings to understand phase transitions in those systems. To shed light on this, we find analytically the diffusion, Reynolds, and swim pressures of a suspension of noninteracting ABPs equipped with inertia (both translational and rotational). Fluid inertia is assumed to be negligible. From this analysis, an enhanced diffusion coefficient due to rotational inertia is obtained. In addition, an alternative effective persistence length and an alternative reorientation time which are sensitive to rotational inertia are also identified. When considering the pressure in this system, it is found that translational and rotational inertia play a role in the swim and Reynolds pressures. All these effects are quantified theoretically and corroborated by performing Langevin dynamics simulations.

This work is organized as follows: Section II describes the employed model. Sections III and IV pose the general equations to solve in order to determine the mean-square displacement (MSD) and the way orientation correlations depending on inertia are found. Sections V and VI present analytical results for the system's MSD and mean-square speed. Section VII presents the calculation of the swim and Reynolds stresses for spherical ABPs embedded in an isotropic environment, and consequently the system's total pressure is revealed. Finally, Sec. VIII validates numerically our analytical results. Conclusions are offered in Sec. IX.

II. PHYSICAL MODEL

Let us study spherical particles of mass M and rotational inertia I that self-propel in a two-dimensional fluctuating environment. This sphere orientation is described by the single rotational degree of freedom $\theta(t)$. In general, the dynamics of this particle is described by its translational velocity, $\mathbf{v}(t)$, and its angular velocity, $\mathbf{\Omega}(t) = \Omega(t)\mathbf{k}$, whose respective Langevin equations are

$$M\frac{d\mathbf{v}}{dt} = -R_U\mathbf{v} + R_U U\mathbf{e} + \mathbf{f}, \quad \frac{d\mathbf{x}}{dt} = \mathbf{v}, \tag{1}$$

$$I\frac{d\Omega}{dt} = -R_\Omega\Omega + g, \quad \frac{d\theta}{dt} = \Omega, \tag{2}$$

where $U(t)$ is the (imposed) swimming speed, $\mathbf{e}(t) = [e_1(t), e_2(t)] = [\cos\theta(t), \sin\theta(t)]$ is the instantaneous unit vector in the direction of swimming with the origin at the center of the sphere, and R_U and R_Ω are respectively the hydrodynamic resistances to translation and rotation. In Eqs. (1) and (2), $\mathbf{f}$ and g are the zero-mean Brownian random force and the torque, whose correlations are given by $\langle f_i(t)f_j(t')\rangle = 2D_T R_U^2\delta_{ij}\delta(t-t')$ and $\langle g(t)g(t')\rangle = 2D_\Omega R_\Omega^2\delta(t-t')$, respectively. Here D_T and D_Ω are the short-time diffusion coefficients (strength of noise), δ_{ij} is the Kronecker's delta, and $\langle\cdot\rangle$ indicates the ensemble average [24].

From Eqs. (1) and (2), one can solve for the instantaneous sphere position, $\mathbf{x}(t)$, the angular orientation, $\theta(t)$, and the velocity, $\mathbf{v}(t)$. Explicitly,

$$\mathbf{x}(t) = \mathbf{x}_0 + \tau_M\mathbf{v}_0(1-e^{-t/\tau_M}) + \frac{1}{R_U}\int_0^t[\mathbf{F}^{\rm swim}(t') + \mathbf{f}(t')][1-e^{-(t-t')/\tau_M}]dt', \tag{3}$$

$$\theta(t) = \theta_0 + \tau_I\Omega_0(1-e^{-t/\tau_I}) + \frac{1}{R_\Omega}\int_0^t[1-e^{-(t-t')/\tau_I}]g(t')dt', \tag{4}$$

$$\mathbf{v}(t) = \mathbf{v}_0 e^{-t/\tau_M} + \frac{1}{M}\int_0^t[\mathbf{F}^{\rm swim}(t') + \mathbf{f}(t')]e^{-(t-t')/\tau_M}dt', \tag{5}$$

where we denote the translational and rotational relaxation times by $\tau_M = M/R_U$ and $\tau_I = I/R_\Omega$. Here $\mathbf{F}^{\rm swim}(t) = R_U U(t)\mathbf{e}(t)$ represents the swimming force, while $\mathbf{x}_0$, θ_0, Ω_0, and $\mathbf{v}_0$ are initial conditions. In what follows and without loss of generality, we set those initial conditions equal to zero.

III. DERIVATION OF EFFECTIVE DIFFUSION

To determine the particle's effective diffusion in two dimensions ($d = 2$), D_E, defined as

$$D_E = \lim_{t\to\infty}\frac{\langle\mathbf{x}(t)\cdot\mathbf{x}(t)\rangle}{(2d)t}, \tag{6}$$

one should find its mean-square displacement $\langle\mathbf{x}(t)\cdot\mathbf{x}(t)\rangle$. To do so, we square Eq. (3) and apply to this result an ensemble average. We finally get

$$\langle\mathbf{x}\cdot\mathbf{x}\rangle = \frac{1}{R_U^2}\int_0^t\int_0^t[\langle\mathbf{F}^{\rm swim}(t'')\cdot\mathbf{F}^{\rm swim}(t')\rangle(1-e^{-(t-t'')/\tau_M} - e^{-(t-t')/\tau_M} + e^{-(2t-t'-t'')/\tau_M})]dt'dt'' + \frac{1}{R_U^2}\int_0^t\int_0^t[\langle\mathbf{f}(t'')\cdot\mathbf{f}(t')\rangle(1-e^{-(t-t'')/\tau_M} - e^{-(t-t')/\tau_M} + e^{-(2t-t'-t'')/\tau_M})]dt'dt'', \tag{7}$$

where we used the fact that random translational forces and swimming forces are not correlated.

IV. ORIENTATION CORRELATION FUNCTIONS

From Eq. (7), one notices that in order to evaluate $\langle\mathbf{x}\cdot\mathbf{x}\rangle$, we have to explicitly determine the correlations in swimmer orientations. One way to achieve this is to recall that Eq. (2) represents an Ornstein-Uhlenbeck process whose respective probability density function (PDF) obeys the so-called Kramers equation [25], $\partial P/\partial t = -\Omega\partial P/\partial\theta + \tau_I^{-1}\partial P/\partial\Omega + D_\Omega/\tau_I^2\partial P^2/\partial\Omega^2$, and whose solution, $P(\theta,\Omega,t|\theta',\Omega',t')$, may be integrated to find the needed marginal PDFs and finally to calculate integrals of the form $\langle\cos\theta\cos\theta'\rangle =$

$\iint d\theta d\theta' \cos\theta \cos\theta' P(\theta, t|\theta', t')P(\theta, t)$. Alternatively, and using the fact that Eq. (2) is a Gaussian process, it is possible to show that [26]

$$\begin{aligned}&\langle \cos\theta(t_2)\cos\theta(t_1)\rangle \\ &= \tfrac{1}{2}\mathrm{Re}\big[e^{i\langle\Delta\theta\rangle-\frac{1}{2}[\langle\Delta\theta^2\rangle-\langle\Delta\theta\rangle^2]}\big] \\ &\quad + \tfrac{1}{2}\mathrm{Re}\big[e^{i\langle\Delta\theta+2\theta(t_1)\rangle-\frac{1}{2}[\langle[\Delta\theta+2\theta(t_1)]^2\rangle-\langle\Delta\theta+2\theta(t_1)\rangle^2]}\big], \end{aligned} \tag{8}$$

where $\Delta\theta = \theta(t_2) - \theta(t_1)$ and $\mathrm{Re}(\cdot)$ stands for the real part. Thus by solving the indicated averages in Eq. (8) and using that $\theta(t)$ is a centered Gaussian and stationary process, together with the orientational symmetry in this problem, the swimming direction correlations are finally obtained as

$$\langle \mathbf{e}(t)\cdot\mathbf{e}(t_1)\rangle = e^{-S_R[\frac{1}{\tau_I}(t-t_1)-1+e^{-\frac{1}{\tau_I}(t-t_1)}]}, \tag{9}$$

where the rotational Stokes number $S_R = \tau_I/\tau_R$ ($\tau_R = 1/D_\Omega$) has been introduced. As one can see, by setting $\tau_I \to 0$ ($I \to 0$) in the latter correlations, we recover the classical Brownian exponential decay in two dimensions, $\langle \mathbf{e}(t)\cdot\mathbf{e}(t_1)\rangle = e^{-(t-t_1)/\tau_R}$ [24]. Further simulations on the effect of inertia on the orientation correlations are presented in Appendix A.

V. MEAN-SQUARE DISPLACEMENT

Let us now evaluate Eq. (2) for the simplest case of a self-propelled particle swimming at constant speed, $U(t) = U =$ constant, along $\mathbf{e}(t)$. Hence, we substitute Eq. (9) into Eq. (2). After certain algebraic steps, we finally obtain the general formula for the long-time MSD, namely,

$$\langle \mathbf{x}\cdot\mathbf{x}\rangle = \frac{2U^2}{D_\Omega} e^{S_R} S_R^{1-S_R}\Gamma(S_R, 0, S_R)t + 4D_T t, \tag{10}$$

where the generalized incomplete Gamma function $\Gamma(a, b, c) = \int_b^c q^{a-1}e^{-q}dq$ has been introduced. Classical linear diffusion in time is once again observed. The contribution from self-propulsion is quadratic in its speed but with an extra coefficient, $C = e^{S_R}S_R^{1-S_R}\Gamma(S_R, 0, S_R) \geqslant 1$ [see Fig. 3(b)], which depends on the rotational Stokes number. Notice that the long-time MSD grows as rotational inertia increases. Setting $U = 0$ in Eq. (10) gives us the MSD result for passive particles. To validate Eq. (10), Langevin dynamics simulations were performed and the results are discussed in Sec. VIII. Finally, by taking the limit $S_R \to 0$, Eq. (10) reduces to the well-known long-time MSD expression of overdamped ABPs, namely, $\langle \mathbf{x}\cdot\mathbf{x}\rangle = (2U^2/D_\Omega)t + 4D_T t$.

Effective diffusivity

Let us now find the effective diffusivity (D_E) for the case of a self-propelled particle swimming at constant speed, $U(t) = U$, along $\mathbf{e}(t)$. Using Eq. (6) together with Eq. (10) leads to

$$D_E = \frac{U^2}{2D_\Omega} e^{S_R} S_R^{1-S_R}\Gamma(S_R, 0, S_R) + D_T. \tag{11}$$

As it can be seen, there is another mechanism for enhancing ABPs' effective diffusion. By adding rotational inertia ($S_R \neq 0$) to active particles, one finds an increment in the swimmers' diffusion. This contribution was not previously observed since an overdamped model was frequently proposed. To explain this enhanced diffusion, one should notice that when keeping inertia, the time an ABP takes to rotate due to external random perturbations (reorientation time, $\langle t_{\mathrm{re}}\rangle$) will increase (compared to τ_R) due to inertia, and as a consequence, its persistence length ($L_E = U\langle t_{\mathrm{re}}\rangle$) will also grow (see Fig. 1). Furthermore, using the following definition of reorientation time, $\langle t_{\mathrm{re}}\rangle = \int_0^\infty \langle \mathbf{e}(t)\cdot\mathbf{e}(t_1)\rangle d\tau$, where $\tau = t - t_1$, together with Eq. (9), we find an expression for this effective reorientation time, namely,

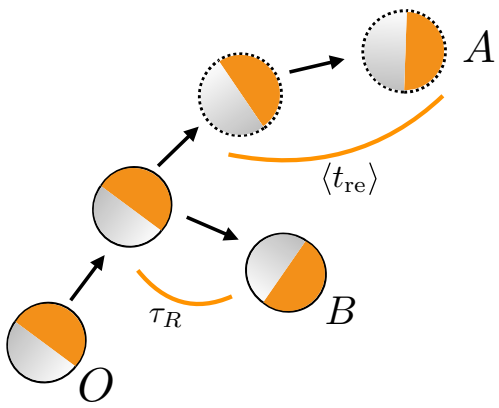

FIG. 1. Paths a swimmer can take depending on its rotational inertia. Path *OB*: A swimmer with no rotational inertia will change its direction in time τ_R. Path *OA*: Due to rotational inertia, the particle is turning slower; hence it will displace further than path *OB*.

$$\langle t_{\mathrm{re}}\rangle = \frac{e^{S_R}}{D_\Omega} S_R^{1-S_R}\Gamma(S_R, 0, S_R), \tag{12}$$

which behaves asymptotically, for S_R large, as $\langle t_{\mathrm{re}}\rangle \sim \tau_R\sqrt{S_R}$. Notice that for zero rotational inertia ($S_R = 0$), Eq. (12) reduces to the classical reorientation time $\langle t_{\mathrm{re}}\rangle = \tau_R$. Given Eq. (12), one can also find an effective persistence length, which for this case is

$$L_E = \frac{U e^{S_R}}{D_\Omega} S_R^{1-S_R}\Gamma(S_R, 0, S_R). \tag{13}$$

Using these generalized effective length and time scales, one can write (assuming D_T is small with respect to activity) Eq. (11) as $D_E = L_E^2/2\langle t_{\mathrm{re}}\rangle$, which for the overdamped case becomes $D_E = l^2/2\tau_R$, where $L_E > l = U\tau_R$ and $\langle t_{\mathrm{re}}\rangle > \tau_R$. Note that by taking the limit $S_R \to 0$ to Eq. (11), one recovers the classical effective diffusion coefficient $D_E = U^2/2D_\Omega + D_T$.

VI. MEAN-SQUARE SPEED

A very important quantity in statistical mechanics is the particles' average translational kinetic energy $\langle K\rangle$. Let us calculate $\langle K\rangle$ for the case of active Brownian particles with both translational and rotational inertia. By using Eq. (1), it is possible to show that

$$\mathbf{v} = \mathbf{v}_0 e^{-t/\tau_M} + \frac{1}{M}\int_0^t [\mathbf{F}^{\mathrm{swim}}(t') + \mathbf{f}(t')]e^{-(t-t')/\tau_M}dt'; \tag{14}$$

hence using a procedure similar to Eq. (2), together with the orientational correlation Eq. (9), and after certain algebraic steps, one finally gets the following for long times:

$$\langle \mathbf{v}\cdot\mathbf{v}\rangle = \frac{U^2 e^{S_R}}{S_T}\left(\frac{1}{S_R}\right)^{\frac{S_R}{S_T}+S_R-1}\Gamma\left(\frac{S_R}{S_T}+S_R,0,S_R\right), + \frac{2D_T R_U}{M}, \tag{15}$$

where the translational Stokes number, $S_T = \tau_M/\tau_R$ ($\tau_R = 1/D_\Omega$), has been introduced. In this case, the mean-square speed depends on both rotational (S_R) and translational (S_T) inertia. Note that the mean-square speed of passive particles only depends on translational inertia. Additionally, if we consider an active system with only translational inertia, we can take the limit $S_R \to 0$ to the latter equation to obtain

$$\langle \mathbf{v}\cdot\mathbf{v}\rangle = \frac{U^2}{1+S_T} + \frac{2D_T R_U}{M}. \tag{16}$$

Using Eq. (16) and by defining an average kinetic energy $\langle K\rangle = (M/2)\langle \mathbf{v}\cdot\mathbf{v}\rangle$, one finds that the kinetic energy for the latter system is $\langle K\rangle = MU^2/[2(1+S_T] + D_T R_U$, which this time depends on the mass of the particle. This does not occur for a passive Brownian particle with translational inertia. For this passive system and in two dimensions, Eq. (16) indicates that $\langle K\rangle = D_T R_U$. This result points to the following observation: Inertial effects in the kinetic energy are present only when activity is considered (activity couples translation and rotation). This is in accordance with the results of Takatori and Brady [21], where inertial effects appear in the Reynolds stress only when there is activity in the system. In fact, by using Eq. (16) and the definition of the Reynolds stress, we recover Eq. (25) (a term purely from inertial effects) from the following section.

To validate Eqs. (15) and (16), Langevin dynamics simulations were performed and the results are discussed in Sec. VIII.

VII. SWIM AND REYNOLDS PRESSURE

Let us find the effect of inertia on the bulk properties of our system by calculating its swim and Reynolds pressures.

A. Swim pressure

The swim stress, $\boldsymbol{\sigma}^{\text{swim}}$, is defined as [9]

$$\boldsymbol{\sigma}^{\text{swim}} = -n\langle \mathbf{x}(t)\mathbf{F}^{\text{swim}}(t)\rangle, \tag{17}$$

where n is the number of particles per unit area. Using Eq. (3) (with $\mathbf{x}_0 = 0$ and $\mathbf{v}_0 = 0$), together with the definition of the swimming force, and after applying ensemble average, we obtain

$$\boldsymbol{\sigma}^{\text{swim}} = -\frac{n}{R_U}\int_0^t \left\langle \mathbf{F}^{\text{swim}}(t)\mathbf{F}^{\text{swim}}(t')\right\rangle \times (1-e^{-(t-t')/\tau_M})dt', \tag{18}$$

where the fact that random translational forces and swimming forces are not correlated has been used.

Let us now evaluate Eq. (18) for the simplest case of a self-propelled particle swimming at constant speed, $U(t) = U =$ constant, along $\mathbf{e}(t)$, and immersed in an isotropic environment. We then substitute Eq. (9) into Eq. (18), and after certain algebraic steps, we finally obtain the general formula for the long-time swim stress, namely,

$$\frac{\boldsymbol{\sigma}^{\text{swim}}}{nk_sT_s} = -e^{S_R}S_R^{1-S_R}\Gamma(S_R,0,S_R)\mathbf{I} + e^{S_R}\left(\frac{1}{S_R}\right)^{\frac{S_R}{S_T}+S_R-1}\Gamma\left(\frac{S_R}{S_T}+S_R,0,S_R\right)\mathbf{I}, \tag{19}$$

where $S_T = \tau_M/\tau_R$ ($\tau_R = 1/D_\Omega$) is the translational Stokes number, $\Gamma(a,b,c) = \int_b^c q^{a-1}e^{-q}dq$ represents the generalized incomplete Gamma function, and $k_sT_s = R_U U^2/2D_\Omega$. By taking the limit $S_R \to 0$, one can reduce Eq. (19) to

$$\boldsymbol{\sigma}^{\text{swim}} = -\frac{nk_sT_s}{1+S_T}\mathbf{I}. \tag{20}$$

Equation (20) indicates that as translational inertia increases, the swim stress decreases. From Fig. 3, one can observe that Eq. (19) shows a dependence on S_T similar to that of Eq. (20).

Note that Eq. (20) is exactly the same as in Ref. [21], with only a constant difference due to the dimensionality considered. To validate Eq. (19), Langevin dynamics simulations were performed and the results are discussed in Sec. VIII.

Finally, by using Eq. (19) together with the definition $\Pi^{\text{swim}} = -\text{tr}(\boldsymbol{\sigma}^{\text{swim}})/2$ (here tr represents the trace), one obtains the analytical expression for the swim pressure in the system, namely,

$$\frac{\Pi^{\text{swim}}}{nk_sT_s} = e^{S_R}S_R^{1-S_R}\Gamma(S_R,0,S_R) - e^{S_R}\left(\frac{1}{S^R}\right)^{\frac{S_R}{S_T}+S_R-1}\Gamma\left(\frac{S_R}{S_T}+S_R,0,S_R\right). \tag{21}$$

From the behavior of the right-hand side of Eq. (21) (see Fig. 3), we conclude that another mechanism for enhancing the ABPs' swim pressure has been shown. By adding rotational inertia ($S_R \neq 0$) to active particles, one finds an increment in the swimmers' swim pressure. This contribution was not previously observed since an overdamped model was frequently proposed. Thus for the case of self-propelled particles, rotational inertia plays an important role because activity now couples rotation and translation. In other words, as one adds rotational inertia, the particles' persistence length will increase, thus enhancing their momentum and hence the pressure in the system. The behavior of the swim pressure is shown in Sec. VIII. It is interesting to mention that using Eq. (21), and taking the limit $S_R \to 0$, one recovers the swim pressure of a system with only translational inertia [21] as

$$\frac{\Pi^{\text{swim}}}{nk_sT_s} = \frac{1}{1+S_T}. \tag{22}$$

It can be seen that as translational inertia increases, the swim pressure in the system decreases. This can be explained by observing that as one increases the mass of an active particle, its inertia originates that the particle translates in a different direction with respect to the direction of its swimming force. This diminishes the correlation between $\mathbf{x}$ and $\mathbf{F}^{\text{swim}}$ (the definition of the swim stress), hence the magnitude of the swim pressure.

B. Reynolds pressure

Another important quantity is the Reynolds stress defined as [21] $\boldsymbol{\sigma}^{\mathrm{Rey}} = -nM\langle \mathbf{v}(t)\mathbf{v}(t)\rangle$. Using Eq. (5), it is possible to show that

$$\begin{aligned}\boldsymbol{\sigma}^{\mathrm{Rey}} = &-\frac{n}{M}\int_0^t\int_0^t \langle \mathbf{F}^{\mathrm{swim}}(t'')\mathbf{F}^{\mathrm{swim}}(t')\rangle \\ &\times e^{-(2t-t''-t')/\tau_M}dt''dt' \\ &-\frac{n}{M}\int_0^t\int_0^t \langle \mathbf{f}(t'')\mathbf{f}(t')\rangle \\ &\times e^{-(2t-t''-t')/\tau_M}dt''dt'. \end{aligned} \tag{23}$$

Note that the latter expression is valid for any swimming kinematics. In particular, let us find the Reynolds stress for the present system which considers $U(t) = U =$ constant. Using Eq. (23) together with Eq. (9), and after certain algebraic steps, we obtain

$$\begin{aligned}\boldsymbol{\sigma}^{\mathrm{Rey}} = &-nk_sT_se^{S_R}\left(\frac{1}{S_R}\right)^{\frac{S_R}{S_T}+S_R-1}\Gamma\left(\frac{S_R}{S_T}+S_R,0,S_R\right)\mathbf{I} \\ &-nD_TR_U\mathbf{I}. \end{aligned} \tag{24}$$

We see that the Reynolds stress for ABPs depends on both rotational (S_R) and translational (S_T) inertia. Additionally, in the limit $S_R \to 0$, the latter equation becomes

$$\boldsymbol{\sigma}^{\mathrm{Rey}} = -\frac{nk_sT_s}{1+1/S_T}\mathbf{I} - nD_TR_U\mathbf{I}, \tag{25}$$

which is exactly the same as in Ref. [21] but with a constant difference due to the dimensionality considered. Using Eq. (24) and by defining the Reynolds pressure $\Pi^{\mathrm{Rey}} = -tr(\boldsymbol{\sigma}^{\mathrm{Rey}})/2$, one finds that the Reynolds pressure is

$$\begin{aligned}\Pi^{\mathrm{Rey}} = &nk_sT_se^{S_R}\left(\frac{1}{S_R}\right)^{\frac{S_R}{S_T}+S_R-1}\Gamma\left(\frac{S_R}{S_T}+S_R,0,S_R\right) \\ &+nD_TR_U, \end{aligned} \tag{26}$$

which this time depends on both translational and rotational inertia. In addition, for $S_R \to 0$, the latter equation reduces to

$$\Pi^{\mathrm{Rey}} = \frac{nk_sT_s}{1+1/S_T} + nD_TR_U, \tag{27}$$

indicating that as the translational Stokes number increases, the Reynolds pressure in the system also increases [21]. In this case, as inertia grows, the mean-square speed (MSS) in the system decreases [$\langle \mathbf{v}\cdot\mathbf{v}\rangle = U^2/(1+S_T)$]. However, the kinetic energy depends on both the MSS and the mass. The product between the MSS and the mass results in an enhancement of the kinetic energy of the system, hence an increment in the Reynolds pressure. From Fig. 3, one can observe that Eq. (26) shows a dependence on S_T similar to that of Eq. (27).

C. Total pressure

By adding Eqs. (21) and (26), the total pressure in the system is

$$\Pi^{\mathrm{swim}} + \Pi^{\mathrm{Rey}} = nk_sT_se^{S_R}S_R^{1-S_R}\Gamma(S_R,0,S_R) + nD_TR_U. \tag{28}$$

The latter result indicates that the total pressure is independent from the translational Stokes number. One can also see that by setting the swimming speed equal to zero, the classic osmotic pressure is recovered. Note that in the limit $S_R \to 0$, Eq. (28) simplifies to

$$\Pi^{\mathrm{swim}} + \Pi^{\mathrm{Rey}} = nk_sT_s + nD_TR_U, \tag{29}$$

which is a previously reported result [21]. Note that in order to validate Eqs. (21), (26), and (28), Langevin dynamics simulations were performed and the results are discussed in the following section. Before closing this section, consider Eq. (1), multiply it by $\mathbf{x}$, and perform an ensemble average. After these few steps, we get

$$M\frac{d\langle \mathbf{vx}\rangle}{dt} - M\langle \mathbf{vv}\rangle - \langle \mathbf{xF}^{\mathrm{swim}}\rangle = -R_U\langle \mathbf{vx}\rangle + \langle \mathbf{xf}\rangle. \tag{30}$$

Using that for an isotropic medium $(d/dt)\langle \mathbf{xx}\rangle = 2\langle \mathbf{vx}\rangle$, and the fact that $\langle \mathbf{xf}\rangle = \mathbf{0}$, the latter equation simplifies to

$$-M\langle \mathbf{vv}\rangle - \langle \mathbf{xF}^{\mathrm{swim}}\rangle = -\frac{R_U}{2}\frac{d}{dt}\langle \mathbf{xx}\rangle. \tag{31}$$

Finally, by multiplying the latter expression by the number density, and recalling the definition of the swim and Reynolds stresses, one gets

$$\boldsymbol{\sigma}^{\mathrm{Rey}} + \boldsymbol{\sigma}^{\mathrm{swim}} = -nR_U\mathbf{D}, \tag{32}$$

where $\mathbf{D} = \lim_{t\to\infty}\langle \mathbf{xx}\rangle/2t$ represents the diffusion tensor. Expression (32) gives us an important result, that is, the possibility of measuring the total pressure in the system by only obtaining its mean-square displacement. The measurement of the MSD is surely easier than explicitly calculating the pressure. Therefore, Eq. (32) may facilitate experimental work. In addition, this equation indicates that although both stresses depend on the translational and rotational inertia, their sum will only be affected by the rotational Stokes number since diffusion, as indicated by Eq. (11), does so. Notice that Eq. (32) can be confirmed by our previous results. For example, adding the swim and Reynolds stresses [Eqs. (19) and (24)], we immediately obtain the right-hand side of Eq. (32). This equation will further lead to a general expression for the total pressure in a two-dimensional system, $\Pi^{\mathrm{tot}} = \Pi^{\mathrm{swim}} + \Pi^{\mathrm{Rey}}$, namely,

$$\Pi^{\mathrm{tot}} = \frac{nR_U}{2}\mathrm{tr}(\mathbf{D}). \tag{33}$$

In the following section, Eq. (28) is also validated numerically.

VIII. LANGEVIN DYNAMICS SIMULATIONS

In order to verify our analytical results, we compare them with Langevin dynamics simulations (see Appendix B for further information). We thus introduce the dimensionless variables $\widetilde{\mathbf{x}} = \mathbf{x}/l$, $\widetilde{t} = t/\tau_R$, and $\widetilde{\mathbf{v}} = \mathbf{v}/U$. In this way, the system can be characterized by the Peclet number $\mathrm{Pe} = U^2\tau_R/D_T$, which compares advection (due to activity) and diffusion. For the case of the diffusion analysis, we fix $S_T = 0.82$ and $\mathrm{Pe} = 690$ (similar to typical experiments dealing with catalytic particles [15,27,28]), whereas for the case of the swim and Reynolds pressure simulations, the translational Stokes number varies in the range $S_T = [0.082, 100]$

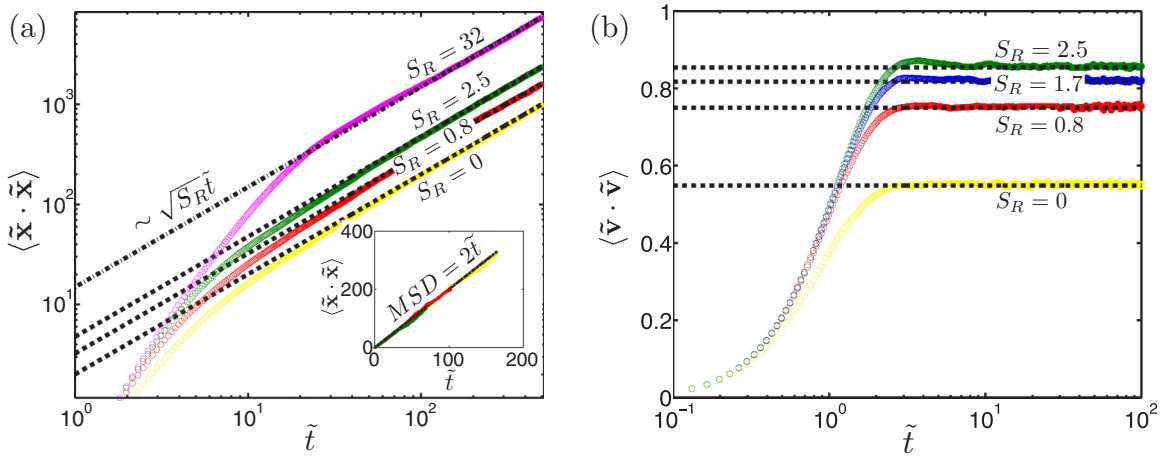

FIG. 2. Comparison between theoretical results (black dashed lines) and Langevin dynamics simulations (circles) of a system of noninteracting ABPs with inertia. Here, $\mathrm{Pe} = U^2\tau_R/D_T = 690$ and $S_T = 0.82$. (a) Theoretical and numerical results for the mean-square displacement of a system with different rotational Stokes numbers, namely, $S_R = \{0, 0.8, 2.5, 32\}$. Note the asymptotic behavior (MSD $\sim\sqrt{S_R\tilde{t}}$) for large S_R. This figure shows that the overall diffusivity increases as the rotational inertia increases. In the inset, using a proper scaling, all the MSDs collapse to one curve. (b) Theoretical and numerical results for the mean-square speed of a system with four different rotational Stokes numbers, namely, $S_R = \{0, 0.8, 1.7, 2.5\}$. This figure shows that the overall mean-square speed increases as rotational inertia increases.

while keeping the same Peclet number. The present system is equipped with five different rotational Stokes numbers, namely, $S_R = \{0, 0.8, 1.7, 2.5, 32\}$. To perform the ensemble averages, between 20 000 to 50 000 realizations were considered. The mean-square displacement and speed results are illustrated in Fig. 2, where the mean-square displacement (shown as solid lines) for four different rotational Stokes numbers, together with the theoretical result given by Eq. (10) (shown as dashed lines) are plotted in Fig. 2(a). This figure shows that the overall diffusion coefficient is enhanced as the rotational inertia increases in the system. For reference, the classical (inertia neglected) enhanced diffusion constant, $D = D_T + U^2/2D_\Omega$, is shown as the black dashed line with $S_R = 0$. The other asymptotic limit for large S_R ($S_R = 32$ in our simulations) is also illustrated as a dashed-dotted black line. Figure 2(a) also shows an excellent quantitative agreement between the numerical results and our analytical predictions. Note that one can also render the system's variables adimensional as $\tilde{\mathbf{x}} = \mathbf{x}/L_E$, $\tilde{t} = t/\langle t_{\mathrm{re}}\rangle$. By doing so, the Peclet number would be $\mathrm{Pe} = U^2\langle t_{\mathrm{re}}\rangle/D_T$, which is now affected by the rotational Stokes number; therefore for the present experiment one has five different Peclet's numbers, namely: $\mathrm{Pe}(S_R = 0) = 690$, $\mathrm{Pe}(S_R = 0.8) = 1117$, $\mathrm{Pe}(S_R = 1.7) = 1409$, $\mathrm{Pe}(S_R = 2.5) = 1645$, and $\mathrm{Pe}(S_R = 32) = 6428$. This indicates that as S_R increases, advection in the system also grows. Using the latter scaling, all the MSDs collapse to the function $\mathrm{MSD} = 2\tilde{t}$ as indicated in the inset of Fig. 2(a). Under the same conditions as Fig. 2(a), we calculate numerically

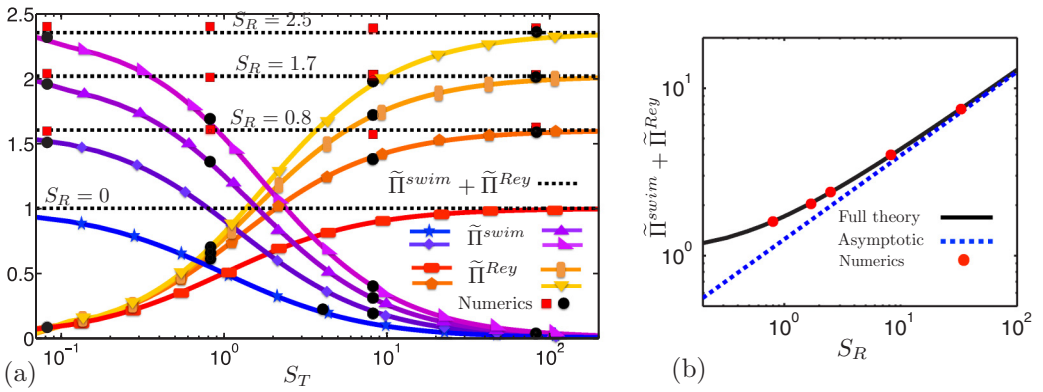

FIG. 3. Pressure of a system of noninteracting ABPs with inertia equipped with $\mathrm{Pe} = U^2\tau_R/D_T = 690$ and $S_T = [0.082, 100]$. (a) Comparison between theoretical results (solid and black dashed lines) and Langevin dynamics simulations (circles and squares) of the dimensionless swim and Reynolds pressures. This figure shows the way both swim and Reynolds pressures depend on translational (S_T) and rotational (S_R) inertia. (b) Dimensionless total pressure in the system as a function of the rotational Stokes number. The full expression [Eq. (28)] is plotted as a black solid line. For large S_R, its asymptotic value is $\widetilde{\Pi}^{\mathrm{swim}} + \widetilde{\Pi}^{\mathrm{Rey}} \simeq \sqrt{\pi S_R/2}$ (blue dashed line). Langevin dynamics simulation data appear as red circles.

the mean-square speed of the system and compare it to our theoretical expressions given by Eqs. (15) and (16). This is shown in Fig. 2(b), where Langevin simulation data are shown as red circles, while the theoretical expressions [Eqs. (15) and (16)] are shown as dashed black lines. Once again an excellent agreement between theory and simulations is observed. For the swim and Reynolds pressures, Langevin simulation results are illustrated in Fig. 3(a). In this figure, the dimensionless swim pressure ($\widetilde{\Pi}^{\rm swim} = \Pi^{\rm swim}/nk_sT_s$), the Reynolds pressure ($\widetilde{\Pi}^{\rm Rey} = \Pi^{\rm Rey}/nk_sT_s$), and the sum of both ($\widetilde{\Pi}^{\rm swim} + \widetilde{\Pi}^{\rm Rey}$) are plotted as a function of the translational Stokes number. The theoretical results given by Eqs. (21) and (26) are shown as solid lines with their respective symbols, whereas Eq. (28) is shown as black dashed lines. Langevin dynamics simulation results are shown as black circles and red squares. One can see an excellent agreement between theory and simulations which validates our theoretical predictions. Surprisingly, both swim and Reynolds stresses are sensitive to translational and rotational inertia; however, their sum ($\widetilde{\Pi}^{\rm swim} + \widetilde{\Pi}^{\rm Rey}$) does not depend on translational inertia. This result confirms our previous theoretical prediction given by Eq. (32). In addition, Fig. 3(b) shows the behavior of $\widetilde{\Pi}^{\rm swim} + \widetilde{\Pi}^{\rm Rey}$ [according to Eq. (28) and shown as a black solid line] as a function of the rotational Stokes number.

It is worth mentioning that for large S_R, one can find an asymptotic behavior to Eq. (28), which gives in a more explicit way its dependence on S_R. After certain steps, we get

$$\widetilde{\Pi}^{\rm swim} + \widetilde{\Pi}^{\rm Rey} \simeq \sqrt{\pi S_R/2}. \tag{34}$$

This asymptotic result is plotted as a blue dashed line in Fig. 3(b). Langevin simulation results appear as red circles.

IX. CONCLUDING REMARKS

In this work we found theoretically the effect of translational and rotational inertia on the diffusion, swim, and Reynolds pressures of a system of spherical noninteracting ABPs, thus generalizing previous overdamped models. Taking into account the inertia contribution in the orientation correlations enabled us to obtain analytical expressions for the system's effective diffusion coefficient, as well as for its mean-square speed. These expressions revealed that rotational inertia leads in general to an enhancement of both diffusion and mean-square speed. To explain this enhancement, one should notice that rotational inertia increases the reorientation time of active particles (thus allowing the particles to travel longer distances before changing direction). This fact led us to define an alternative effective reorientation time as well as an alternative persistence length. Afterwards, and to see the effect of inertia on bulk properties, the calculation of the total pressure for this system was carried out. This showed that the presence of inertia also leads to an enhancement (asymptotically proportional to the square root of the rotational inertia) of both the swim and Reynolds pressures. These results are also expected to be relevant when explaining phase transitions in a system of inertial ABPs.

All the theoretical findings reported here were corroborated by performing Langevin dynamics simulations showing an excellent agreement between theory and numerical experiments.

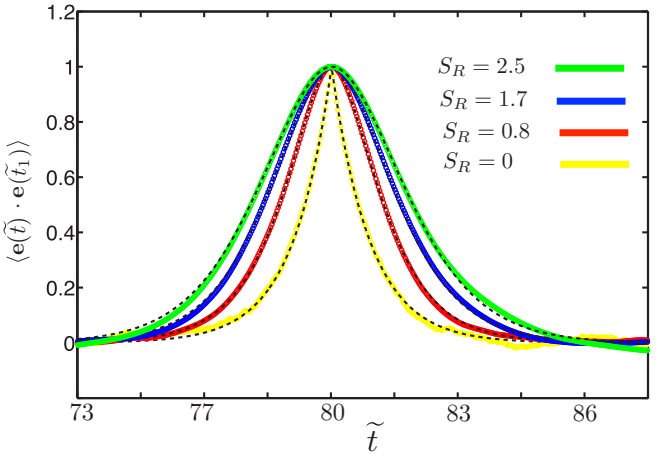

FIG. 4. Effect of inertia on the orientation correlation. The figure shows a comparison between the theoretical results given by Eq. (9) (black dashed lines) and Langevin dynamics simulations (solid lines). Here $t_1 = 80$. The classical result for $S_R = 0$, $\langle \mathbf{e}(t) \cdot \mathbf{e}(t_1) \rangle = e^{-(t-t_1)/\tau_R}$, can be seen as the yellow solid line.

ACKNOWLEDGMENT

M.S. thanks Consejo Nacional de Ciencia y Tecnologia, CONACyT, for support under Grant No. CB 2014/237848.

APPENDIX A: ORIENTATION CORRELATIONS

To explicitly illustrate the effect of rotational inertia (S_R) on the behavior of $\langle \mathbf{e}(t) \cdot \mathbf{e}(t_1) \rangle$, we plot in Fig. 4, for $S_R = \{0, 0.8, 1.7.2.5\}$ and $\widetilde{t}_1 = 80$, the theoretical expression (black dashed lines) given by Eq. (9),

$$\langle \mathbf{e}(t) \cdot \mathbf{e}(t_1) \rangle = e^{-S_R[\frac{1}{\tau_I}(t-t_1)-1+e^{-\frac{1}{\tau_I}(t-t_1)}]},$$

as a function of time. We then superpose our Langevin dynamics simulations (solid lines) for the orientation correlation to show an excellent agreement between theory and simulations. As one can see, by setting $S_R \to 0$ ($I \to 0$) in Fig. 4, we recover the classical exponential decay in two dimensions, $\langle \mathbf{e}(t) \cdot \mathbf{e}(t_1) \rangle = e^{-(t-t_1)/\tau_R}$. Its numerical simulation appears as the yellow solid line.

APPENDIX B: VERLET-TYPE ALGORITHM FOR LANGEVIN DYNAMICS

To specify the numerical method we used, consider the following definitions: $r=\{x, y, \theta\}$, $v=\{v_x, v_y, \Omega\}$, $m=\{M, I\}$, $\beta=\{f_x, f_y, g\}$, $\alpha=\{R_T, R_\Omega\}$, and $f(r, t)$ as an external force or torque. Therefore, we can express the components of Eqs. (1) and (2) as

$$m\frac{dv}{dt} = f(r,t) - \alpha v(t) + \beta(t), \qquad \frac{dr}{dt} = v, \tag{B1}$$

Following Ref. [29] and by introducing the discrete time $t_n = n\Delta t$, it is possible to build a second-order accuracy method in the time step Δt for Eq. (B1). The discretization of system

(B1) according to Ref. [29] is

$$r(t_n+\Delta t) = r(t_n) + bv(t_n)\Delta t + f(t_n)\frac{b\Delta t^2}{2m} + \beta(t_n+\Delta t)\frac{b\Delta t}{2m}, \tag{B2}$$

$$v(t_n+\Delta t) = av(t_n) + [af(t_n) + f(t_n+\Delta t)]\frac{\Delta t}{2m} + \beta(t_n+\Delta t)\frac{b}{m}, \tag{B3}$$

where

$$a = \frac{1-\alpha\Delta t/2m}{1+\alpha\Delta t/2m}, \quad b = \frac{1}{1+\alpha\Delta t/2m}, \tag{B4}$$

the Gaussian random number $\beta(t_n+\Delta t)$ satisfies $\langle\beta(t_n)\rangle = 0$, and $\langle\beta(t_n)\beta(t_m)\rangle = 2D_kR_k^2\Delta t\delta_{nm}$. Here $k=\{T,\Omega\}$ is an index representing either translational (T) or rotational (Ω) motion. Note that setting $\{\alpha,\beta\}=0$ in Eqs. (B2) and (B3) leads to

$$r(t_n+\Delta t) = r(t_n) + v(t_n)\Delta t + f(t_n)\frac{b\Delta t^2}{2m}, \tag{B5}$$

$$v(t_n+\Delta t) = av(t_n) + [f(t_n) + f(t_n+\Delta t)]\frac{\Delta t}{2m}, \tag{B6}$$

which is the classical velocity Verlet scheme. Equations (B2) and (B3) were employed to perform the Langevin dynamics simulations in this work. For our simulations, we chose the time step $\Delta\widetilde{t} = 0.01$ and we performed between 20 000 to 50 000 realizations to calculate the respective ensemble averages.

[1] M. C. Marchetti, J. F. Joanny, S. Ramaswamy, T. B. Liverpool, J. Prost, M. Rao, and R. A. Simha, Rev. Mod. Phys. **85**, 1143 (2013).
[2] S. Ebbens, Curr. Opin. Colloid Interface Sci. **21**, 14 (2016).
[3] C. Bechinger, R. D. Leonardo, H. Löwen, C. Reichhardt, G. Volpe, and G. Volpe, Rev. Mod. Phys. **88**, 045006 (2016).
[4] M. F. Hagan and A. Baskaran, Curr. Opin. Cell Biol. **38**, 74 (2016).
[5] S. C. Takatori and J. F. Brady, Curr. Opin. Colloid Interface Sci. **21**, 24 (2016).
[6] I. Theurkauff, C. Cottin-Bizonne, J. Palacci, C. Ybert, and L. Bocquet, Phys. Rev. Lett. **108**, 268303 (2012).
[7] F. Ginot, I. Theurkauff, D. Levis, C. Ybert, L. Bocquet, L. Berthier, and C. Cottin-Bizonne, Phys. Rev. X **5**, 011004 (2015).
[8] J. Stenhammar, A. Tiribocchi, R. J. Allen, D. Marenduzzo, and M. E. Cates, Phys. Rev. Lett. **111**, 145702 (2013).
[9] S. C. Takatori, W. Yan, and J. F. Brady, Phys. Rev. Lett. **113**, 028103 (2014).
[10] A. P. Solon, Y. Fily, A. Baskaran, M. E. Cates, Y. Kafri, M. Kardar, and J. Tailleur, Nat. Phys. **11**, 673 (2015).
[11] J. Li, B. Esteban-Fernández de Ávila, W. Gao, L. Zhang, and J. Wang, Sci. Rob. **2**, eaam6431 (2017).
[12] R. Stocker and W. M. Durham, Science **325**, 400 (2009).
[13] X. Yang, M. L. Manning, and M. C. Marchetti, Soft Matter **10**, 6477 (2014).
[14] S. C. Takatori and J. F. Brady, Phys. Rev. E **91**, 032117 (2015).
[15] S. Ebbens, R. A. L. Jones, A. J. Ryan, R. Golestanian, and J. R. Howse, Phys. Rev. E **82**, 015304(R) (2010).
[16] T. Speck and R. L. Jack, Phys. Rev. E **93**, 062605 (2016).
[17] S. A. Mallory, A. Šarić, C. Valeriani, and A. Cacciuto, Phys. Rev. E **89**, 052303 (2014).
[18] R. G. Winkler, A. Wysocki, and G. Gompper, Soft Matter **11**, 6680 (2015).
[19] A. P. Solon, J. Stenhammar, R. Wittkowski, M. Kardar, Y. Kafri, M. E. Cates, and J. Tailleur, Phys. Rev. Lett. **114**, 198301 (2015).
[20] M. Joyeux and E. Bertin, Phys. Rev. E **93**, 032605 (2016).
[21] S. C. Takatori and J. F. Brady, Phys. Rev. Fluids **2**, 094305 (2017).
[22] Y. Fily, Y. Kafri, A. P. Solon, J. Tailleur, and A. Turner, J. Phys. A: Math. Theor. **51**, 044003 (2018).
[23] C. Scholz, S. Jahanshahi, A. Ldov, and H. Lowen, Nat. Commun. **9**, 1 (2018).
[24] M. Doi and S. Edwards, *The Theory of Polymer Dynamics* (Clarendon, Oxford, England, 1999).
[25] H. Risken and T. Frank, *The Fokker-Planck Equation* (Springer, Berlin, 1996).
[26] W. Coffey, Y. Kalmikov, and Y. Valdron, *The Langevin Equation: With Applications in Physics, Chemistry and Electrical Engineering* (World Scientific, Singapore, 1996).
[27] S. C. Takatori, R. De Dier, J. Vermant, and J. F. Brady, Nat. Commun. **7**, 10694 (2016).
[28] J. R. Howse, R. A. L. Jones, A. J. Ryan, T. Gough, R. Vafabakhsh, and R. Golestanian, Phys. Rev. Lett. **99**, 048102 (2007).
[29] N. Graznbech-Jensen and O. Farago, Mol. Phys. **111**, 983 (2013).